RSC Advances

PAPER

View Article Online
View Journal | View Issue

Cite this: *RSC Adv.*, 2025, **15**, 4220

Enhanced adsorption of Congo red onto camphor leaf-derived biosorbents modified with lanthanum

Peng Gao, *[a] Yue Zhuo[b] and Guodong Sun[c]

A novel high-performance porous carbon material, lanthanum(III)-doped camphor leaf-derived porous carbon (La/CPC), was synthesized and used as an adsorbent for the anionic dye Congo red (CR). The La/CPC composite was characterized by nitrogen adsorption and desorption isotherms, scanning electron microscopy, transmission electron microscopy and X-ray photoelectron spectroscopy. The adsorption performance of CR by the CPC and La/CPC composites with different contents of lanthanum(III) was evaluated in fixed-bed breakthrough experiments and batch tests at room temperature (298 K). The La/CPC composite had a high CR uptake capacity, which was found to be superior to those previously reported for other adsorbents. The La/CPC sorbents could be easily regenerated using an ethanol elution technique, and after five cycles, the reused La/CPC sorbent maintained about 98% of its CR capacity. The adsorption kinetics of CR onto the lanthanum(III)-doped CPC sorbent followed a pseudo-second-order kinetic model and fitted well with a Langmuir adsorption isotherm. La/CPC is a promising adsorbent for the removal of anionic dyes from wastewater.

Received 23rd November 2024
Accepted 17th January 2025

DOI: 10.1039/d4ra08315f

rsc.li/rsc-advances

1. Introduction

Porous carbons are the most popular sorbent materials for the removal of pollutants from wastewater,[1,2] and they are particularly effective for the removal of a large variety of dyes from wastewater, making them excellent alternatives to other expensive treatment options. However, porous carbons possess several disadvantages, such as non-selectivity and ineffectiveness for vat dyes.[3,4] In addition, most carbon-based adsorbents are derived from relatively expensive starting materials, which makes them costly. These problems have inspired the search for low-cost and highly selective adsorbents.

Ideally, precursors for porous carbons should be readily available, inexpensive and non-hazardous in nature. In recent years, a number of inexpensive agro-waste materials, such as rice husks,[5] groundnut shells,[6] orange peels,[7] sawdust,[8] rice straw,[9] soybean hulls,[10] waste apricots,[11] degreased coffee beans,[12] lemon peels,[13] de-oiled soya,[14] and other natural products[15,16] have been used to remove anionic dyes from wastewater. The advantage of using waste resources is that it saves disposal costs and helps alleviate potential environmental problems.

The camphor tree, also known as camphor laurel, is an evergreen plant that belongs to the laurel family. It grows natively in the valleys and mountains of Japan, China, Taiwan and Vietnam. Camphor leaves (CLs) are bright green, heart-shaped leaves that are about 7 cm long and 3.5 cm wide (Fig. 1). Camphor leaves are porous and contain various organic compounds. In addition, they are abundantly available. Thus, CLs should be an optimal precursor for the preparation of inexpensive porous carbon materials (camphor leaf-based porous carbons, CPCs).

Recently, a great deal of research has focused on improving the selectivity of porous carbon materials by modifying their properties to give them an affinity for specific dyes. For example, effective adsorbents have been developed for methyl orange,[17] Congo red,[18] rhodamine B,[19] malachite green,[20] methylene

Fig. 1 Shape and size of a camphor leaf.

[a]*School of Mechanical and Intelligent Manufacturing, Jiujiang University, Jiujiang, 332005, China. E-mail: 15781807@qq.com*

[b]*Technology Department of Library, Jiujiang University, Jiujiang, 332005, China*

[c]*School of Materials Science and Engineering, Jiujiang University, Jiujiang, 332005, China*

blue,[21] and orange II.[22] In most of these cases, the surface chemistry and the pore structure of the material play a role in the specific application.[23]

Porous carbons with controlled porosities and defined surface properties have been widely used as supports for the adsorption and separation of anionic dyes.[18] The fabrication of these adsorbents involves the initial preparation of a porous carbon material followed by impregnation with a metal ion salt, which is sometimes then reduced to the metallic state.[18] This impregnation procedure results in metallic nanoparticles in the pores. Charge attractions between the metal ions and the anionic dye greatly improve the selectivity and the adsorption capacity of the porous carbon for the anionic dye.[24,25] However, these types of adsorbents still face major problems, such as poor selectivity and low uptake capacities for some dyes, and they are difficult to recycle.[26]

To the best of our knowledge, there are no studies that have investigated the effects of doping lanthanum(III) metal ions on the adsorption of dyes by porous carbon materials. In order to obtain porous carbons with high selectivity and capacities, these types of studies are critical. Therefore, in this work, camphor leaf-derived adsorbents modified with different amounts of lanthanum(III) were synthesized and characterized. Their performance as adsorbents in the removal of Congo red (a typical anionic dye) from aqueous solutions was tested. Adsorptive breakthrough curves (dynamic tests) and batch tests (static tests) were both conducted in order to study the adsorption and desorption performances of these new carbon materials.

2. Experimental

2.1 Materials

Camphor leaves were collected from the campus of Jiujiang University, Jiujiang, China. Potassium hydroxide and lanthanum(III) chloride were purchased from Sigma Chemical Company (St. Louis, Mo., USA). High-purity nitrogen (99.995%) was provided by Jiujiang Xinheyuan Gas Co., Ltd, Jiujiang, China. All other reagents were of analytical reagent grade.

2.2 Preparation of porous carbons

The procedure to prepare the CPCs has been described previously.[1,3] Briefly, the camphor leaves were first washed with deionized water to remove dirt from their surfaces and were then dried overnight in an oven at 378 K. The dried leaves were cut and sieved into pieces of ~200 μm and then mixed with KOH (KOH/CL mass ratio = 4/1). The resulting mixture was placed into a horizontal pipe reactor (50 mm o.d.). The temperature of the reactor was increased to the activation temperature (973 K) at a heating rate of 1 K min^{-1}. During the carbonization process, high-purity nitrogen (99.99%) was flowed through the reactor at a flow rate of 30 mL min^{-1}. Finally, the sample was cooled to room temperature. The samples were then washed with deionized water until the pH of the filtrate was neutral. The final samples (CPCs) were obtained by heating the samples at 393 K under vacuum for 24 h.

2.3 Modification of the porous carbons

An incipient wetness technique was used to impregnate the CPCs with an aqueous solution of lanthanum(III) chloride. The required amounts of lanthanum(III) chloride to achieve lanthanum(III) loadings of 0.3, 0.5, 0.8, and 1 mmol were calculated, and the CPCs were immersed in the corresponding La solution for 24 hours. After impregnation, the adsorbents were dried at 373 K for 5 h and then heated in a nitrogen atmosphere at 973 K for 3 h. The obtained samples are denoted as La3/CPC, La5/CPC, La8/CPC and La10/CPC, where the number represents the concentration of the La(III) impregnation solution in mmol.

2.4 Sample characterization

The characterization of the pore structures of the samples was performed using low-temperature nitrogen adsorption–desorption isotherms measured using an automated adsorption apparatus (Micromeritics, ASAP 2020). The materials were pre-treated *in situ* under vacuum at 573 K. The surface area was calculated by the BET method (the relative pressure p/p_0 range for the BET calculations was 0.005–0.2). For TEM measurements, powdered samples were deposited on a grid with a perforated carbon film and transferred onto a JEOL2100F electron microscope operating at 80 kV. The SEM images were obtained using a scanning electron microscope made by PHILIPS (Netherlands) with a working distance of 14 mm, an accelerating voltage of 15 kV and digital image recording. The influence of La(III)-related defects on the electronic structure of the La/CPC surfaces was studied by X-ray photoelectron spectroscopy (XPS, ESCALAB 250Xi).

2.5 Adsorption studies

A series of CR solutions with concentrations ranging from 50 to 1200 mg L^{-1} were prepared by dissolving an appropriate amount of dye in deionized water. In each batch experiment, 20 mg of adsorbent was suspended in 50 mL of the dye solution. First, the time dependence of the CR adsorption for each type of adsorbent was investigated to determine the time required for adsorption equilibrium. During the adsorption experiments, the mixtures were continuously shaken in a shaking bath at a constant temperature (298 K). At the end of the adsorption, the samples were filtered and the residual concentrations of CR in the filtrate were determined using a UV-visible spectrophotometer (Thermo Fisher Evolution 300 PC) at the maximum wavelength of 497 nm. The calibration curves were very reproducible and there was a linear relationship between the concentration range used and the absorbance. The adsorbed amount of CR at equilibrium, q_e (mg g^{-1}), was calculated as follows:

$$q_e = \frac{(C_o - C_e)\cdot V}{W} \quad (1)$$

where C_o and C_e (mg L^{-1}) are the initial and equilibrium concentrations of the CR solution, respectively, V (L) is the volume of solution, and W (g) is the weight of the adsorbents used. All experiments were conducted in duplicate, and the

Table 1 Different isotherm models and their linear forms

Isotherm	Nonlinear form	Linear form	Plot	Equation
Langmuir-I	$q_e = \frac{K_L C_e}{1 + K_L C_e}$	$\frac{C_e}{q_e} = \frac{1}{q_L \cdot K_L} + \left(\frac{1}{q_L}\right) \cdot C_e$	$\frac{C_e}{q_e}$ *versus* C_e	(2)
Freundlich	$q_e = K_f C_e^{\frac{1}{n}}$	$\ln q_e = \ln K_f + \left(\frac{1}{n}\right) \cdot \ln C_e$	$\ln q_e$ *versus* $\ln C_e$	(3)
D–R	$q_e = q_s e^{(-K_D \varepsilon^2)}$	$\ln q_e = \ln q_s - K_D \varepsilon^2$	$\ln q_e$ *versus* ε^2	(4)

average values are reported. The average deviation of the duplicate results was found to be within ±1%.

The linear forms or a Langmuir isotherm model,[27] Freundlich model[28] and D–R model[4] were used to study the adsorption performance of the adsorbents. These equations are presented in Table 1.where q_m is the maximum capacity of adsorption expressed in mg g^{-1}; K_L is a constant related to the affinity of the binding sites in L mg^{-1}; 'K_f' and 'n' are the measures of adsorption capacity and the intensity of adsorption, respectively; $\beta = (RT)/b_T$ is the Temkin constant; T is the absolute temperature in K; R is the universal gas constant; q_s is the D–R isotherm constant in mg g^{-1}; and ε represents the Polanyi potential constant in kJ mol^{-1}; $\varepsilon = RT\ln\left(1 + \frac{1}{C_e}\right)$.

2.6 Breakthrough experiments

The adsorption performance of the La/CPC sorbent was tested using breakthrough curves. The experiments to collect the breakthrough curves were performed in a vertical quartz column (length = 300 mm; inner diameter = 10 mm) with a glass grid for supporting the adsorbent. The adsorption materials (~5 g) were loaded into the adsorption column inside a glove box to avoid contact with air. The CR solution was delivered with a mini creep pump (BT01-YZ1515, Zhejiang Nade Company, China). Prior to each adsorption measurement, the adsorbent was activated by heating to 473 K for 2 h in a stream of nitrogen. After cooling to room temperature (298 K) in a stream of nitrogen, the sorbent was consolidated by lightly tapping the column.

The adsorption experiments were conducted at 298 K and atmospheric pressure. First, the fixed bed was flushed downward with deionized water at a flow rate of 0.2 cm^3 min^{-1} for 30 min, and then the feed was switched to the CR solution at the same flow rate. The samples were taken at regular intervals to examine the CR content in the solutions until saturation was reached. Breakthrough curves were obtained by plotting the transient CR concentration *versus* the cumulative solution volume. The concentrations were normalized with the total CR content in the feed, and the cumulative solution volumes were normalized with the volume of the adsorbent bed. The normalized CR adsorption capacity of the adsorbents was calculated using the following equations:

$$q_b = \left(\frac{v\rho x_i}{m}\right) \times t_b \quad (5)$$

$$q_s = \left(\frac{v\rho x_i}{m}\right) \int_0^{t_s} \left[1 - \frac{c_t}{c_i}\right] dt \quad (6)$$

where q_b is the breakthrough capacity per unit mass of adsorbent, mg g^{-1}; q_s is the saturation capacity of unit mass of adsorbent, mg g^{-1}; v is the flow rate of CR solution, cm^3 min^{-1}; ρ is the CR solution density, g cm^{-3}; c_i is the initial CR content, mg L^{-1}; c_t is the CR concentration of the solution passing through the bed at time t, mg L^{-1}; m is the mass of adsorbent in the column, g; x_i is the CR concentration of solution, mg L^{-1}; t_b is the breakthrough time, min; and t_s is the saturation time when $c_t/c_i = 1$, min.

A pseudo-first-order model,[1] a pseudo-second-order model,[3] and an intra-particle diffusion model[4] were used to analyze the kinetic data. These models can be expressed as follows:

Pseudo-first-order model:

$$\ln(q_e - q_t) = \ln(q_e) - K_1 t \quad (7)$$

Pseudo-second-order model:

$$\frac{t}{q_t} = \frac{1}{K_2 q_e} + \frac{t}{q_e} \quad (8)$$

Intra-particle diffusion model:

$$q_t = K_3 t^{1/2} \quad (9)$$

where q_e and q_t (mg g^{-1}) are the uptakes of CR at equilibrium and at time t (min), respectively, K_1 (1 min^{-1}) is the adsorption rate constant, K_2 (g mg^{-1} min^{-1}) is the rate constant for the second-order equation, and K_3 (mg g^{-1} $min^{-1/2}$) is the intra-particle diffusion rate constant. In order to quantitatively compare the applicability of different kinetic models, a normalized standard deviation, Δq (%), was calculated as follows:

$$\Delta q(\%) = \frac{\left(q_{e,exp} - q_{e,cal}\right)}{q_{e,exp}} \times 100\% \quad (10)$$

3. Results and discussion

3.1 Material characterization

The nitrogen adsorption isotherms and pore size distribution of CPC, La3/CPC, La5/CPC, La8/CPC and La10/CPC at77 K are shown in Fig. 2(a and b), respectively. According to the IUPAC classification, all the samples exhibit Type I adsorption isotherms, which are characteristic of microporous materials, as reported in the literature.[2,17] The properties of the adsorbents are given in Table 2. The BET surface area and the total pore

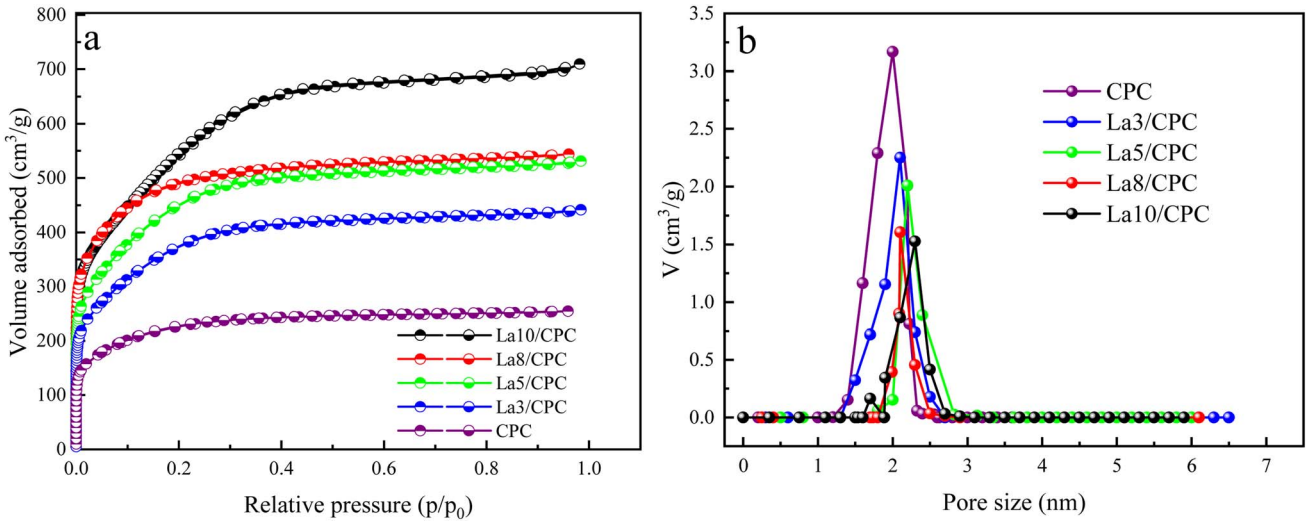

Fig. 2 N_2 adsorption isotherms of CPCs before and after modification with lanthanum (a), and pore size distributions of CPCs before and after modification with lanthanum (b).

Table 2 Structural properties of the adsorbents

Samples	S_{BET} ($m^2\ g^{-1}$)	S_{mic} ($m^2\ g^{-1}$)	S_{meso} ($m^2\ g^{-1}$)	V_{total} ($cm^3\ g^{-1}$)	V_{meso} ($cm^3\ g^{-1}$, %)	V_{mic} ($cm^3\ g^{-1}$, %)	Average pore diameter (nm)
CPC	1949	1845	104	1.10	0.37, 34	0.73, 66	1.98
La3/CPC	1826	1634	101	1.06	0.45, 42	0.61, 58	2.11
La5/CPC	1621	1443	96	0.95	0.41, 43	0.54, 57	2.21
La8/CPC	1342	1259	83	0.92	0.41, 45	0.51, 55	2.28
La10/CPC	828	764	64	0.90	0.42, 47	0.48, 53	2.31

volume of CPC were 1949 $m^2\ g^{-1}$ and 1.10 $cm^3\ g^{-1}$, respectively. Adding La decreased both the BET surface area and the total pore volume, and higher La loadings resulted in larger decreases (*i.e.* the surface area and total pore volume for La10/CPC were the smallest, 828 $m^2\ g^{-1}$ and 0.90 $cm^3\ g^{-1}$ respectively). The pore size distributions were determined by density functional theory calculations, and the pore sizes of the CPC and La/CPC samples were all between 1.4 and 2.8 nm. A t-plot analysis of pore distribution shows that the microporous surface areas of the samples decreased and the percent of mesopores increased with the increase in the amounts of La. This suggests that the La modifications preferentially occur at the openings of the micropores and small mesopores, and are probably due to the high potential fields in the small pores and the easy attachment that can occur at the pore openings.[17] As a result, the La nanoparticles expanded the micropores in the CPC samples and transformed them into small mesopores in the La/MPC structures. The relatively high surface areas of CPC and the La/CPC materials should provide huge capacities for the adsorption of dye molecules inside the pore structure.

SEM was used to investigate the surface image and the results for La8/CPC samples are shown in Fig. 3(a). The image

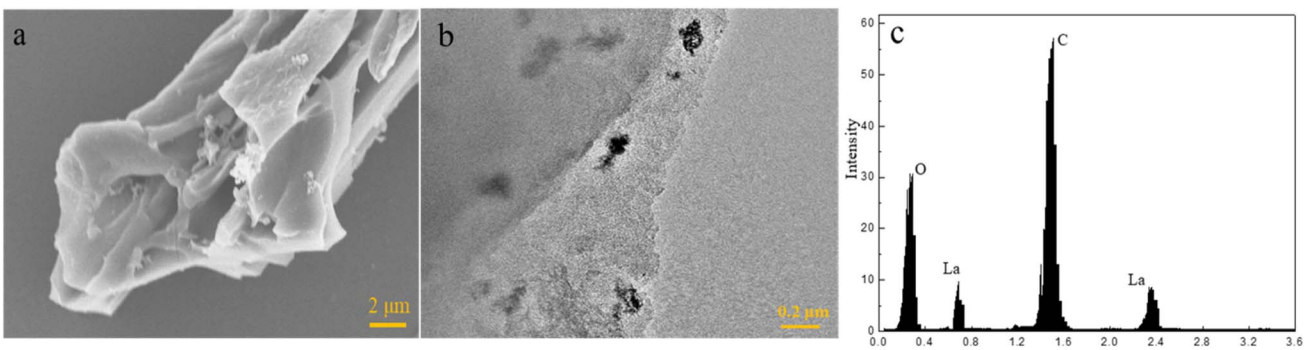

Fig. 3 SEM image of the La8/CPC sample (a), TEM image of the La8/CPC sample (b), and EDS spectrum of the La8/CPC sample (c).

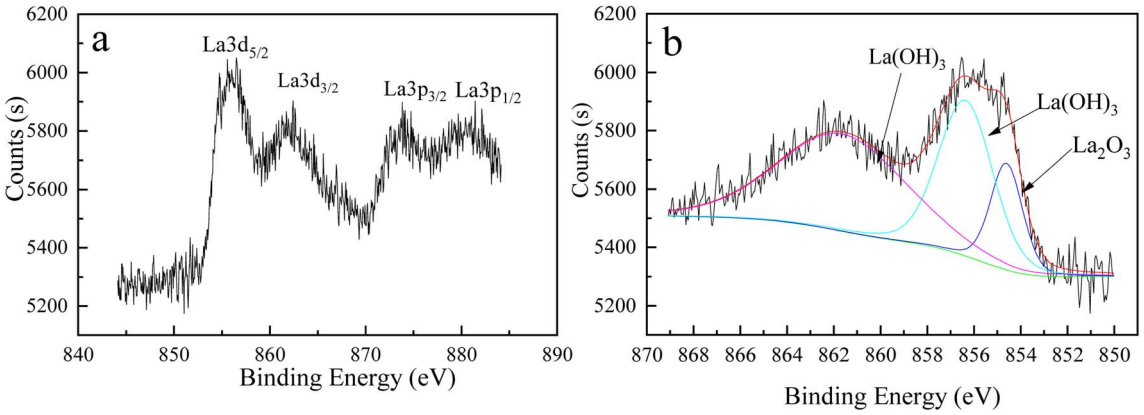

Fig. 4 La-XPS spectra of the La8/CPC sample (a and b).

shows that the sample contains cavities and rough surfaces, which are due to the carbon material preparation process.[1,17] The result also proved that the La/CPC composite will be enhanced by the presence of more porosity, which can hold more dye molecules from the solution during adsorption. No impurities were detected in the nanostructures. To further investigate the pore structure and image, TEM was also used to study the samples, and the results are shown in Fig. 3(b). The TEM result shows that some of the carbon material surface appears to be covered with a metal coating. EDS was used to verify the elemental compositions of the La8/CPC sample, and the results are shown in Fig. 3(c). Only three elements, namely, C, O and La were found.

In order to obtain information about the surface of the La-doped carbon, *i.e.* the location and distribution of the La phases on the CPC, XPS analysis was performed, and the results are shown in Fig. 4(a and b). The XPS survey spectra of La8/CPC has four distinct peaks, which are due to La $3d_{5/2}$, La $3d_{3/2}$, and La $3p_{1/2}$. The 3p orbital of Lanthanum (La) in XPS will exhibit a double peak due to spin–orbit splitting, corresponding to La $3p_{1/2}$ and La $3p_{3/2}$. Furthermore, the binding energy of La $3p_{1/2}$ is higher than that of La $3p_{3/2}$. The La $3d_{3/2}$ peaks centered at 855 and 856 eV can be ascribed to La_2O_3 and $La(OH)_3$ respectively.[27,28] The La satellite peaks indicate that the La atoms are present in an oxygen environment. The peak at 861.6 eV is a satellite peak of $La(OH)_3$.[28] The survey XPS spectra corresponding to La $3p_{1/2}$ further confirmed the presence of element La. The La $3p_{3/2}$ XPS peak binding energies of La_2O_3 and $La(OH)_3$ are shifted by about 0.5 eV, which is due to any apparent charging normalized with the C 1s peak set to 284.4 eV. XPS analysis may reveal that certain functional groups in Congo red molecules, such as negatively charged sulfonic groups, interact with the positively charged surface of the La-modified CPC, leading to electrostatic adsorption.[29]

3.2 Adsorption isotherms

The adsorption isotherms of CR at 298 K on CPC before and after modification with La at a solid/liquid ratio of 0.5 g L^{-1} are presented in Fig. 5(a). Normally, the Langmuir isotherm applies to uniformly adsorbed surfaces with uniform adsorption affinity, the Friedrich isotherm is an empirical relationship for adsorption on a non-uniform surface, and the D–R isotherm explains the adsorption process of substances on heterogeneous surfaces, such as microporous or submicroporous materials. The linear forms of Langmuir, Freundlich, and Temkin models are shown in Fig. 5(b–d). The experimental equilibrium adsorption data were then fitted using Langmuir, Freundlich, and D–R isotherm models (eqn (2), (3) and (4)). The calculated constants for these isotherm equations along with the R^2 values (standard deviation) are presented in Table 3. For all the samples, the Langmuir isotherm gave the best fit (R^2 > 0.998). This suggests that the dye adsorption is limited to monolayer coverage and that the surfaces are relatively homogeneous.[28]

The maximum monolayer adsorption capacity (q_L) for CR was the highest for La8/CPC with the capacities decreasing in the following order: La8/CPC > La5/CPC > La10/CPC > La3/CPC > CPC. The La/CPC sorbents adsorb more CR than CPC because of reactions between lanthanum and the CR molecules. However, the capacities are not proportional to the amount of loaded La. This non-linear response could be a result of variations in the structures and compositions of the La/CPC surfaces, or it may be due to the inaccessibility of active La sites for some domains.[28]

The adsorption capacities of the adsorbents in this work and those for some previously reported sorbents are summarized in Table 4. The CR uptake capacities of all the La/CPC sorbents are comparable or superior to those previously reported for activated carbons, zeolites and MOFs.[1,2,18,30–35]

3.3 Adsorption kinetics

The effect of contact time on the CPC and the La/MPC adsorption capacities for CR are shown in Fig. 6(a). To analyze the kinetic data, pseudo-first-order, pseudo-second-order, and intraparticle diffusion models were employed (Fig. 6(c and d)). The adsorption capacities for CR increased with the increase in contact time until adsorption equilibrium occurred within 150 min for all the samples. The capacity is constant when all the parameters are fixed (298 K, 3 h contact time, 1200 mg L^{-1} initial concentration, 7 pH value, and 0.4 g L^{-1} adsorbent dose). With the evolution of time, the uptake or adsorbed amount may

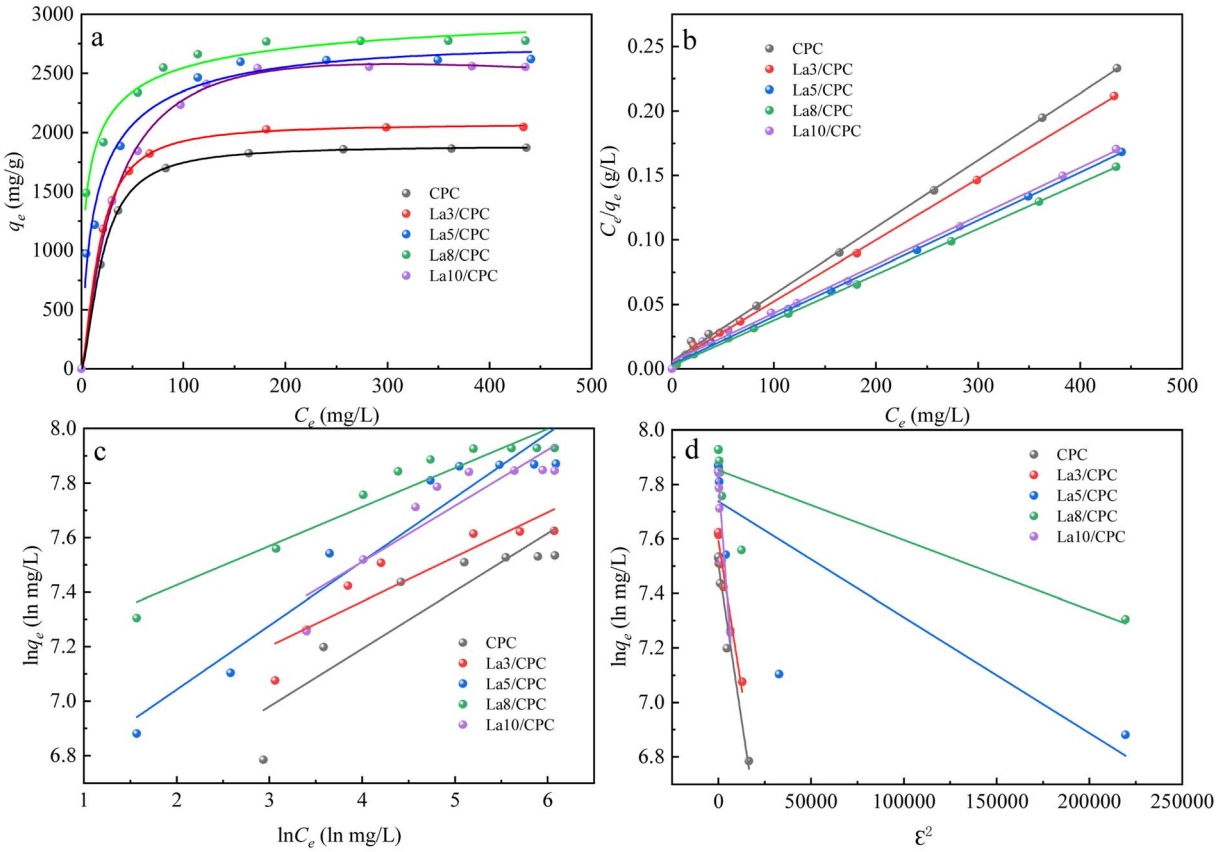

Fig. 5 Adsorption isotherms (a), Langmuir (b), Freundlich (c), and D–R (d) linear adsorption isotherm models of CR on CPC, La3/CPC, La5/CPC, La8/CPC, and La10/CPC samples (t = 4 h, pH = 7, dose = 0.4 g L^{-1}, T = 298 K).

Table 3 Parameters of the isotherm models for the adsorption processes

	Langmuir			Freundlich			D–R		
Samples	q_m (mg g^{-1})	K_L (L mg^{-1})	R^2	K_f (L g^{-1})	n	R^2	q_s (mg g^{-1})	K_D (mol^2 kJ^{-2})	R^2
CPC	1961	0.062	0.999	570	4.721	0.815	7.506	6×10^{-6}	0.975
La3/CPC	2128	0.076	0.999	821	6.111	0.824	7.594	6×10^{-6}	0.966
La5/CPC	2703	0.083	0.999	715	4.255	0.934	7.733	6×10^{-7}	0.687
La8/CPC	2857	0.124	0.999	1260	6.980	0.926	7.851	3×10^{-7}	0.741
La10/CPC	2703	0.048	0.998	803	4.863	0.821	7.821	10^{-5}	0.934

Table 4 Maximum uptake capacities of the CR dye on various adsorbents

Dye	Adsorbent	Maximum uptake capacities (mg g^{-1})	References
CR	CPC	1871	This work
	La8/CPC	2777	This work
	MPC	900	1
	Ni/MPC	1719	1
	Cu-BTC	877	2
	Ni/Cu-BTC	1078	18
	Activated carbon	300	30
	Maghemite nanoparticles	208	31
	Commercial activated carbon	494	32
	Activated carbon	272	33
	Silk cotton carbon	250	34
	White ash	171	35
	Pellet adsorbent	32	35

change. The fast adsorption at the initial stage is probably due to the availability of uncovered surface sites on the adsorbent.

Eqn (7)–(9) were used to calculate the pseudo-first-order, pseudo-second-order, and intra-particle diffusion kinetic constants respectively, and those results along with R^2 values at different temperatures are presented in Table 5. There is a large difference between the pseudo-first-order model's experimental and calculated adsorption capacities. However, high R^2 values (>0.99) were obtained for the linear plot of t/q_t *versus* t, suggesting that the adsorption follows pseudo-second-order adsorption kinetics. If the adsorption process follows an intra-particle diffusion mechanism, then the plot of q_t *versus* $t^{1/2}$ will be linear, and if the plot passes through the origin, the rate-limiting process is due only to the intra-particle diffusion.[1] Otherwise, other mechanisms along with intra-particle

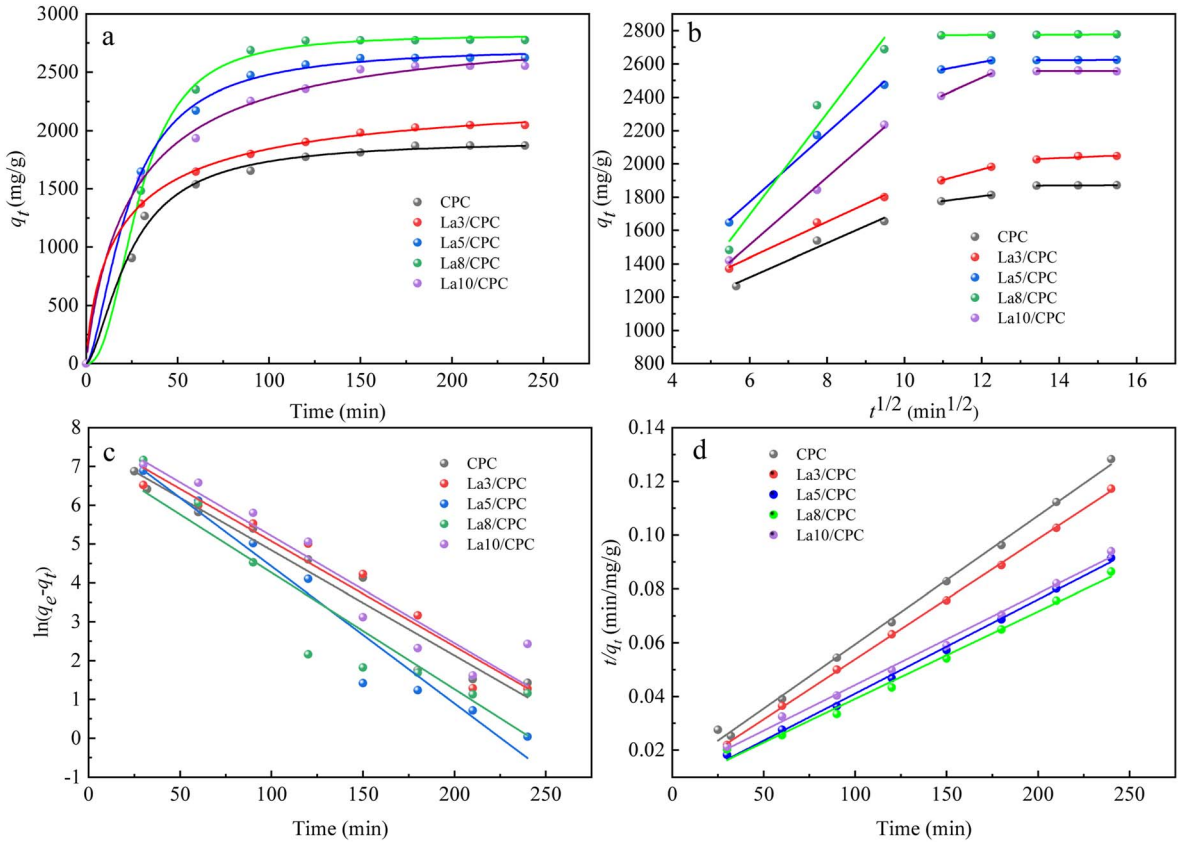

Fig. 6 Adsorption kinetics (a); Weber–Morris intraparticle diffusion plots (b). Pseudo-first-order (c) and pseudo-second-order (d) kinetic models for the adsorption of CR on CPC, La3/CPC, La5/CPC, La8/CPC, and La10/CPC.

Table 5 Kinetic parameters for CR adsorption onto the adsorbents

	Pseudo-first-order rate equation						Pseudo-second-order rate equation					Intra-particle diffusion model		
Adsorbent	$q_{e,exp}$ (mg g^{-1})	$q_{e,cal}$ (mg g^{-1})	K_1 (1/min)	R^2	Δq (mg g^{-1})	Δq (%)	$q_{e,cal}$ (mg g^{-1})	K_2 (g mg^{-1} min^{-1})	R^2	Δq (mg g^{-1})	Δq (%)	C (mg g^{-1})	K_3 (mg g^{-1} min$^{-1/2}$)	R^2
CPC	1871	4040	0.0389	0.890	−2953	12.49	2083	1.987×10^{-5}	0.997	−959	0.85	776	80.24	0.8295
La3/CPC	2046	7921	0.0423	0.727	−6834	28.91	2222	2.230×10^{-5}	0.999	−1097	0.98	1107	66.79	0.9208
La5/CPC	2624	4652	0.0416	0.959	−3565	15.08	2857	2.024×10^{-5}	0.997	−1733	1.54	1428	88.73	0.7699
La8/CPC	2777	4840	0.0468	0.939	−3752	15.87	3125	1.553×10^{-5}	0.992	−2001	1.78	1342	108.10	0.6669
La10/CPC	2554	8942	0.0427	0.911	−7855	33.22	2857	1.424×10^{-5}	0.998	−1733	1.54	1199	97.76	0.8950

diffusion are involved.[1,2] As shown in Fig. 6(b), the plots are not linear over the whole-time range and, instead, can be separated into multi-linear curves, which indicate that the adsorption process has multiple stages. The first line can be attributed to macro-pore diffusion (phase I) and the second linear portion can be attributed to micro-pore diffusion (phase II). These results indicate that the adsorption of CR onto CPC and La/MPC involves more than one process and that intra-particle transport is not the rate-limiting step. This finding is similar to those reported for other carbon materials.[1,3,4,17]

3.4 Breakthrough curves

The CR breakthrough curves of CPC, La3/CPC, La5/CPC, La8/CPC, and La10/CPC are shown in Fig. 7. The shape of the adsorption isotherm provides qualitative insights into the adsorption strength. Specifically, steeper slopes indicate stronger interactions between the adsorbent and the target molecule.[2] In this context, the adsorption curves demonstrate that La/CPC sorbents exhibit stronger interactions with Congo red (CR) compared to CPC alone, suggesting that lanthanum sites enhance CR adsorption. The CR uptake capacity follows the order: La8/CPC > La10/CPC > La5/CPC > La3/CPC. This trend can be attributed to the fact that increasing the amount of lanthanum introduces more active sites for adsorption. However, excessive lanthanum loading may block pores and create diffusion resistance during mass transfer, which can hinder CR uptake. Therefore, La8/CPC, with an optimal lanthanum loading, shows the highest CR adsorption capacity.

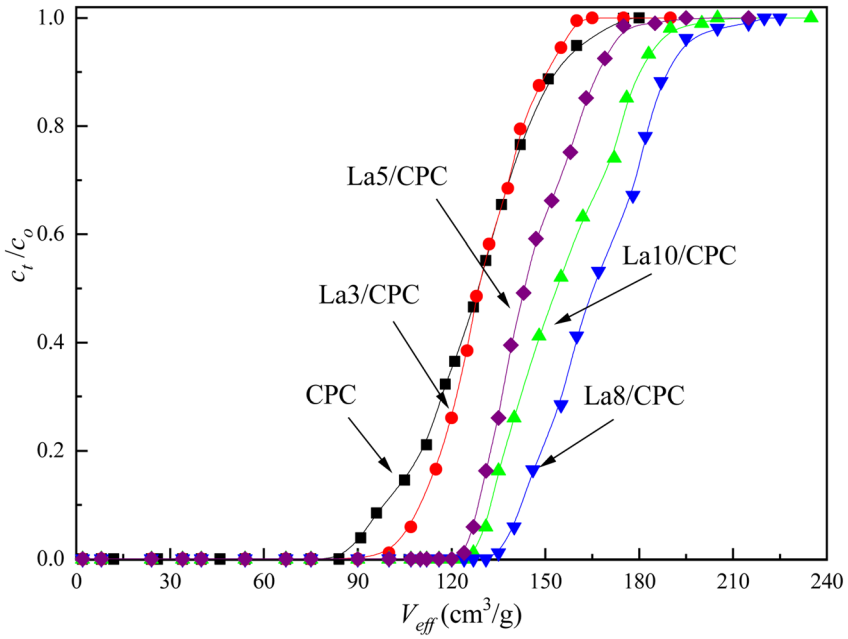

Fig. 7 Breakthrough curves of CR over CPC, La3/CPC, La5/CPC, La8/CPC and La10/CPC.

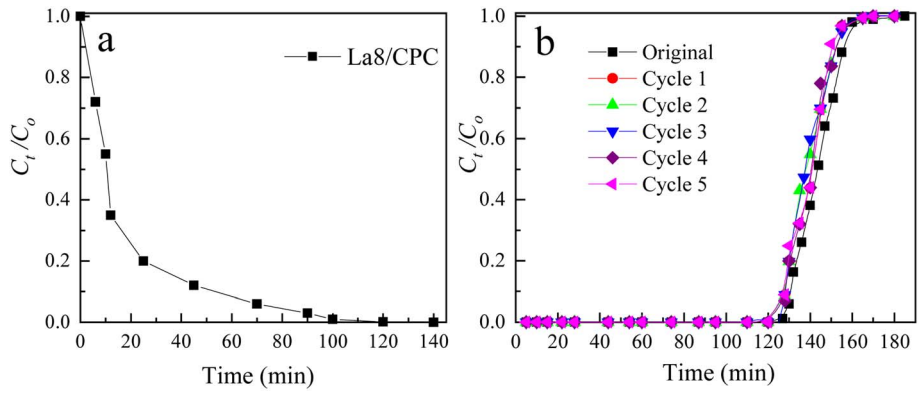

Fig. 8 Desorption curve of CR from La8/CPC in ethanol (a), and the breakthrough curves of CR over La8/CPC for five cycles (b).

3.5 Regeneration tests for La/CPC adsorbents

The recyclability of La/MPC is an important property if the material has to be used for pollution control and environmental protection. An ethanol elution procedure[1,3,4] was used to desorb the CR from the used La8/CPC sample, and the desorption curves are shown in Fig. 8(a). The concentration of CR decreased with time, and the CR was removed from the adsorbents after 2 h. The adsorption performance of the regenerated La/CPC adsorbent was then tested. The CR breakthrough curves for five reuses of regenerated La8/CPC are shown in Fig. 8(b). After five cycles, the CR uptake capacity for the regenerated La8/CPC composite was 2722 mg g^{-1}, which is almost 98% of the initial values. The results show that about 98% of the CR capacity can be recovered after five cycles of reaction, indicating its good recyclability and stability. These results indicate that the La/CPC adsorbent is recyclable and stable.

4. Conclusion

Porous carbons (CPCs) derived from camphor leaves were modified with lanthanum(III) by an impregnation method. The as-prepared adsorbents were characterized by EDS, XPS, nitrogen adsorption/desorption isotherms, SEM and TEM. Compared with CPC, the La/CPCs had lower surface areas and larger pore volumes. The CR adsorption capacities of the La/CPC composite sorbents are comparable to or superior to those previously reported for other carbon-based adsorbents. The adsorption capacity of the La/CPCs increased with the increase in initial CR concentration and with the increase in lanthanum(III) content, which indicates that both physisorption and chemisorption occur during the adsorption process. The equilibrium data are best described by Langmuir isotherms and the adsorption kinetics follow a pseudo-second-order kinetic model. The La/CPC sorbents can be easily regenerated by

ethanol elution and maintain a CR uptake capacity of about 98% after five cycles of regeneration. This study highlights the potential of La/CPC as a highly efficient adsorbent for the removal of anionic dyes from wastewater.

Data availability

The datasets generated and analyzed in the current study are available from the corresponding author upon reasonable request.

Author contributions

Peng Gao wrote the main manuscript text, and Yue Zhuo handled data and regressed formulas. Guodong Sun conducted experiments and organized experimental data. Yue Zhuo and Guodong Sun provided revision suggestions. All authors reviewed the manuscript.

Conflicts of interest

The authors declare that they have no known competing financial interests or personal relationships that could have appeared to influence the work reported in this paper.

Acknowledgements

This work was supported by China Scholarship Council's Young Backbone Teachers' Overseas Training Program (grant number 202310870001) and was supported by the Science and Technology Research Project of Jiangxi Provincial Department of Education (grant number GJJ211821).

References

1 H. J. Yu, T. T. Wang, L. Yu, W. Dai, N. Ma, X. Hu and Y. Wang, *J. Taiwan Inst. Chem. Eng.*, 2016, **64**, 279–284.
2 J. Hu, W. Dai and X. Y. Yan, *Desalin. Water Treat.*, 2016, **57**, 4081–4089.
3 H. J. Yu, T. T. Wang, W. Dai, X. X. Li, X. Hu and N. Ma, *RSC Adv.*, 2015, **5**, 63970–63977.
4 W. Dai, H. J. Yu, N. Ma and X. Y. Yan, *Korean J. Chem. Eng.*, 2015, **32**, 335–341.
5 S. Chowdhury, R. Mishra, P. Saha and P. Kushwaha, *Desalination*, 2011, **265**, 159–168.
6 R. Malik, D. S. Ramteke and S. R. Wate, *Waste Manage.*, 2007, **27**, 1129–1138.
7 K. V. Kumar and K. Porkodi, *Dyes Pigm.*, 2007, **74**, 590–594.
8 B. H. Hameed and M. I. El-Khaiary, *J. Hazard. Mater.*, 2008, **159**, 574–579.
9 B. H. Hameed and M. I. El-Khaiary, *J. Hazard. Mater.*, 2008, **153**, 701–708.
10 R. M. Gong, J. Sun, D. M. Zhang, K. D. Zhong and G. P. Zhu, *Bioresour. Technol.*, 2008, **99**, 4510–4514.
11 Y. Önal, *J. Hazard. Mater.*, 2006, **137**, 1719–1728.
12 M. H. Baek, C. O. Ijagbemi, O. S. Jin and D. S. Kim, *J. Hazard. Mater.*, 2010, **176**, 820–828.
13 K. V. Kumar, *Dyes Pigm.*, 2007, **74**, 595–597.
14 A. Mittal, L. Krishnan and V. K. Gupta, *Sep. Purif. Technol.*, 2005, **43**, 125–133.
15 P. Saha, S. Chowdhury, S. Gupta and I. Kumar, *Chem. Eng. J.*, 2010, **165**, 874–882.
16 A. Mittal, *J. Hazard. Mater.*, 2006, **133**, 196–202.
17 R. Gong, J. J. Ye, W. Dai, X. Y. Yan, J. Hu, X. Hu, S. Li and H. Huang, *Ind. Eng. Chem. Res.*, 2013, **52**, 14297–14303.
18 J. Hu, H. J. Yu, W. Dai, X. Y. Yan, X. Hu and H. Huang, *RSC Adv.*, 2014, **4**, 35124–35130.
19 Y. Dong, H. M. Lin and F. Y. Qu, *Chem. Eng. J.*, 2012, **193–194**, 169–177.
20 Y. Tian, P. Liu, X. F. Wang and H. S. Lin, *Chem. Eng. J.*, 2011, **171**, 1263–1269.
21 A. W. Marczewski, *Appl. Surf. Sci.*, 2010, **256**, 5145–5152.
22 X. M. Peng, D. P. Huang, T. O. Odoom-Wubah, D. F. Fu, J. L. Huang and Q. D. Qin, *J. Colloid Interface Sci.*, 2014, **430**, 272–282.
23 P. A. Bazuła, A. H. Lu, J. J. Nitz and F. Schuth, *Microporous Mesoporous Mater.*, 2008, **108**, 266–275.
24 C. Y. Yin, M. K. Aroua and W. M. A. W. Daudb, *Sep. Purif. Technol.*, 2007, **52**, 403–415.
25 M. T. Yagub, T. K. Sen, S. Afroze and H. M. Ang, *Adv. Colloid Interface Sci.*, 2014, **209**, 172–184.
26 G. Mezohegyi, F. P. van der Zee, J. Font, A. Fortuny and A. J. Fabregat, *Environ. Manage.*, 2012, **102**, 148–164.
27 J. Goscianska, M. Ptaszkowska and R. Pietrzak, *Chem. Eng. J.*, 2015, **270**, 140–149.
28 J. Goscianska, M. Marciniak and R. Pietrzak, *Chem. Eng. J.*, 2014, **247**, 258–264.
29 Y. Jiang, J. Di, Y. Ma, S. Fu, Y. Dong and B. Yuan, *Environ. Sci. Pollut. Res.*, 2023, **30**(23), 63915–63931.
30 M. K. Purkaita, A. Maitib, S. Dasguptab and S. J. Deb, *Hazard. Mater.*, 2007, **145**, 287–295.
31 A. Afkhami and R. J. Moosavi, *Hazard. Mater.*, 2010, **174**, 398–403.
32 K. Nagarethinam and M. Mariappan, *Water, Air, Soil Pollut.*, 2002, **138**, 289–305.
33 Q. Liu, Y. Gao, Y. T. Zhou, N. Tian, G. F. Liang, N. Ma and W. Dai, *J. Chem. Eng. Data*, 2019, **64**, 3323–3330.
34 K. Kadirvelu, M. Kavipriya, C. Karthika, M. Radhika, N. Vennilamani and S. Pattabhi, *Bioresource. Technol.*, 2003, **87**, 129–132.
35 K. S. Chou, J. C. Tsai and C. T. Lo, *Bioresource. Technol.*, 2001, **78**, 217–219.